Analysis of the short Term-Station Blackout accident at the Peach Bottom Unit-2 reactor with ASTEC including the estimation of the radiological impact with JRODOS

Onur Murat [a,*], Victor Sanchez-Espinoza [a], Fabrizio Gabrielli [a], Robert Stieglitz [a], Cesar Queral [b]

[a] Karlsruhe Institute of Technology, Institute for Neutron Physics and Reactor Technology, Hermann-von-Helmholtz-Platz 1, D-76344 Eggenstein-Leopoldshafen, Germany
[b] Universidad Politecnica de Madrid, Ramiro de Maeztu, 7, 28040, Madrid, Spain

A B S T R A C T

Driven by the Fukushima accident, the ASTEC code has been extended with new capabilities to describe the BWR-behavior, especially of the core, during severe accidents with core meltdown. Hence, models for the BWR-typical core components like absorber cross, canister, water rods related to the chemical reactions, material relocation, and radiative heat transfer were added to ASTEC. To evaluate the prediction capability of ASTEC for BWR, a short-term Station Black-out (ST-SBO) severe sequence of the Peach Bottom Unit-2 was selected. The goal is to predict the radiological source term with ASTEC and the subsequent radiological impact using the JRODOS code. For this purpose, the fuel inventory isotope fractions are determined by the ORIGEN-code. It describes the change of the core isotopic composition during the operation. A comparison of selected parameters of the initial in-vessel phase predicted by ASTEC with the ones of MELCOR shows similar results. But the vessel failure times and mass of molten material ejected from the core calculated by ASTEC deviates from the one of MELCOR. ASTEC predicts late oxidation of core structures leading to an accelerated progression of the accident and to an earlier lower head failure compared to the one calculated by MELCOR for the case of CORBH package. After the containment failure in the drywell head flange, the fraction of the nuclide inventory released to the environment predicted by ASTEC are similar to the ones of MELCOR. Finally, JRODOS was used to predict the fission product dispersion and radiological impact around the Peach Bottom Unit-2 plant. The results showed that in the worst-case scenario, a total effective gamma dose rate of 7.2 mSv/h exist.

1. Introduction

The severe accidents in Fukushima Daiichi power plants resulted in large radiological impact emphasizing the importance of an accurate prediction of the radiological source term after severe accidents for the emergency teams in order to initiate the proper countermeasures to minimize the consequences.

The accurate prediction of radiological impact around the site of a NPP after a severe accident with core degradation requires appropriate computational tools for the following areas: a) prediction of the nuclide inventory in the core for a realistic core loading with fuel assemblies burnt at different degree, b) prediction of the integral NPP behavior during the progression of a severe accident and the fission products release in the core, their transport in the primary/secondary circuits and in the containment, c) estimation of the dispersion of the released fission products and their radiological impact on the citizens and environment.

In order to fulfill the first requirement, namely to describe the change of the nuclide inventory due to the fission process in the core, the subsequent radioactive decay and the different interactions of the neutrons with the core materials (capture, absorption, scattering), dedicated codes like ORIGEN are used, in which the Bateman equation is solved.

Various integral codes for severe accidents such as ASTEC (Chatelard, et al., 2016), MELCOR (Humphries, et al., 2017), MAAP (EPRI, 2010), AC^2 (Wielenberg, et al., 2019), SOCRAT (Leonid, et al., 2019), etc. are being developed, improved, and validated worldwide for severe accident simulations in LWRs. They include chemo-physical and mathematical models for the main phenomena occurring during the in-vessel, ex-vessel phases as well as in the containment, describing the release of fission products from the fuel due to the failure of the safety barrier, their behavior in the primary and secondary loops, and in the containment. New capabilities added to ASTEC to describe BWR-specific components in the core (Chatelard, et al., 2017) include rectangular-shaped fuel channel boxes. Simulation of the subchannel geometry enclosing active core regions in the BWR design with physical models including chemical interactions, material degradation and movement and radiative heat transfer, enabling the extension of the ASTEC's capabilities.

Depending on progression of the accident, the integrity of the

* Corresponding author.
E-mail address: onur.murat@partner.kit.edu (O. Murat).

containment may be lost and the loss of the final barrier will result in radiological dispersion to the environment. In order to take timely actions and evaluate countermeasures for such scenarios, tools such as JRODOS (Ievdin, et al., 2010) have been developed to help decision makers. Applying the results of the severe accident codes to the dispersion calculations shows the consequences of the simulations for the safety of the population and the environment.

BWR power plant design includes specific components such as fuel channel boxes and cross type control blades which increases structural mass in the core region. Compared to the design of PWR, the higher amount of zircaloy, stainless steel, and boron carbide in BWR affects the accident progression and core coolability. A larger amount of metallic structures in the core has the potential to accelerate oxidation kinetics and the release of large amounts of energy during severe accidents and reflooding transients. An average French PWR 900 design contains about 20 tons of zircaloy fuel cladding, about 300 kg of stainless-steel absorber cladding, and has the potential to produce 900 kg of hydrogen generated by oxidation reactions in the reactor vessel. On the other hand, the studied ASTEC model of Peach Bottom Unit-2 BWR4 design hosts 34.17 tons of zircaloy fuel cladding with 22.64 tons of zircaloy fuel channel boxes, 1265 kg of stainless-steel absorber cladding, and 1424 kg of boron carbide absorber material. The simulation results with hydrogen production of more than 1800 kg during the oxidation reactions in-vessel shows the severity potential of the larger amount of metallic structures in the core of the BWR. Moreover, the oxidation process for the boron carbide absorber material is strongly exothermic and the hydrogen production capacity is about 6–7 times higher compared to zircaloy (Adroguer, et al., 2003).

The presence of a high proportion of metallic structures is a challenge to core safety, but eutectic interactions between the large proportion of boron carbide absorber material and the stainless steel cladding can also lead to premature core degradation. The evolution of eutectic melt between boron carbide and stainless steel around 1500 K leads to the formation of molten material below the melting point. The movement of the eutectic melt could interact with the Zircaloy fuel channel boxes and the binary system of boron carbide and stainless steel may lead local failures and early reaching of molten material around the fuel rods (Steinbrück, 2010).

The Primary Containment Vessel (PCV) volume of the BWR design is smaller compared to the PWR containment design. To handle severe accident conditions of high pressures and high temperatures, a wet compartment was added to the BWR PCV structure. The inclusion of a large volume of water, called suppression pool in the wetwell, plays the role of a condensation pool for excess heat. Steam discharged from the core is directed through safety relief valves (SRVs) from the steam line to the suppression pool. In the event of severe accidents, when the fuel rods fail and fission products released to the vessel domain, carrier gasses transport the fission products to the suppression pool. Thanks to the absorption capacity of the liquid water, the excess heat is suppressed there and the fission products are retained in the water pool. For this reason, ex-vessel progression of severe accidents will be different in BWR design than standard dry containment atmosphere of PWR design.

The main objective of this study is to simulate a complete severe accident transient, starting with the description of the fuel and ending with the selected accident scenario, including the consideration of the radiological consequences. In this way, the simulation capabilities of the current ASTEC version for BWR design and the obtained results can be evaluated in terms of public safety. Thanks to collaboration between KIT and IRSN, available recent source code was adopted for this study. Selection of the plant was Peach Bottom Unit-2 BWR4 Mark-1 design as Fukushima Daiichi plants. Also, extensive studies on the Peach Bottom and data availability were one of the major factors for choosing the plant design.

It is worth to mention that the ASTEC-capability to describe the in-vessel phase of BWR-cores was validated in the previous study (Murat, et al., 2020) using the QUENCH-20 BWR experiment. This study showed promising results.

The Chapter 2 describes the ASTEC model of the Peach Bottom Unit-2 including core, vessel, containment volumes and cavity and connections between them. Considered physical phenomena in the model described and boundary conditions of the model explained. In the next, Chapter 3 includes fuel depletion calculation with SCALE-Origen code which is adopted in order to employ corresponding fission product inventory with reference study. Results of the selected scenario presented in the Chapter 4 and after that JRODOS implementation concluded the work by taking into account fission product dispersion and levels of dose rate received by the public.

2. Fuel inventory calculation with ORIGEN

Definition of the decay heat and fission product fractions in the core describes how the accident progress in-vessel, ex-vessel and potential environmental and public hazards. In the previous study (Carbajo, 1994), which is publication of the referenced study report (Carbajo, 1993), statement for the burnup level and isotope fraction was made as following; high burnup fuel after long time full power operation. Exact burnup level and isotope fraction values were unclear in order to reproduce fuel inventory for the ASTEC model. For this reason, depletion module of the SCALE V6.2b code system (Wieselquist, et al., 2020), ORIGEN was adopted in order to reproduce comparable results in the previous MELCOR study.

ORIGEN code solves the rate equations in order to calculate generated or depleted isotope concentrations in the fuel resulted by fission, decay or transmutation. Problem dependent cross section libraries are used in the ORIGEN by interpolating pre-generated cross section libraries. Neutron cross section libraries, which is generated by the Scale using by transport codes, can fit any type of fuel configuration and their operating conditions.

Initial fuel loading in Peach Bottom Unit-2 NPP was General Electric 7x7 and one same type of assembly example in ORIGEN was used. Previous study with MELCOR (Carbajo, 1993) also performed with 168.48 tons of fuel materials which is corresponds to the 7x7 assembly type core loading. Average specific power for BWR fuel assemblies used in U.S. recorded as 24 MW/MTU (Hu, et al., 2016) and one assembly model in ORIGEN input has 0.1902 tons of uranium. Corresponding power level 4.5648 MW for one assembly in ORIGEN was defined and burn time period adjusted as 2 years since the exact operational duration is not specified in MELCOR study.

Achieved discharge burnup was 17.5 GWd/t and it was compared with reference databank for BWR fuel assemblies in U.S. (Fig. 2.1). It was found that 7x7 assembly types were in operation between the early 1970 s and 1985, and discharge burnup records during this time period climbs up to about 26 GWd/MTHM. However, not only the 7x7 assembly types but also other types of assemblies in operation after 1975, and especially the 8x8 assembly numbers is almost as many as the 7x7 assembly at the early 1980 s. Therefore, to separate the burnup of 7x7 assemblies from that of other assemblies, one may conclude that the period from the beginning to 1975 may be appropriate time period to consider. The high burnup peak at the beginning is related to fuel assemblies used for research purposes and not used in the power plants. When considering the selected period, the 17.5 GWd/t achieved discharge burnup are within the range of values recorded for the 7x7 BWR fuel assembly type.

The description of the element groups and the selected elements in previous study with MELCOR and the comparison with the ORIGEN V6.2b calculation were presented in Table 2.1. The underlined elements are the selected ones in the reference study and the masses of the selected elements for the reference study and the ORIGEN results were given. The comparison of the selected element masses in Table 2.1 shows that the selected power and the achieved discharged burnup for a period of 2 years produce suitable amount and fraction fission products for the ASTEC ISODOP module.Table 4.1.

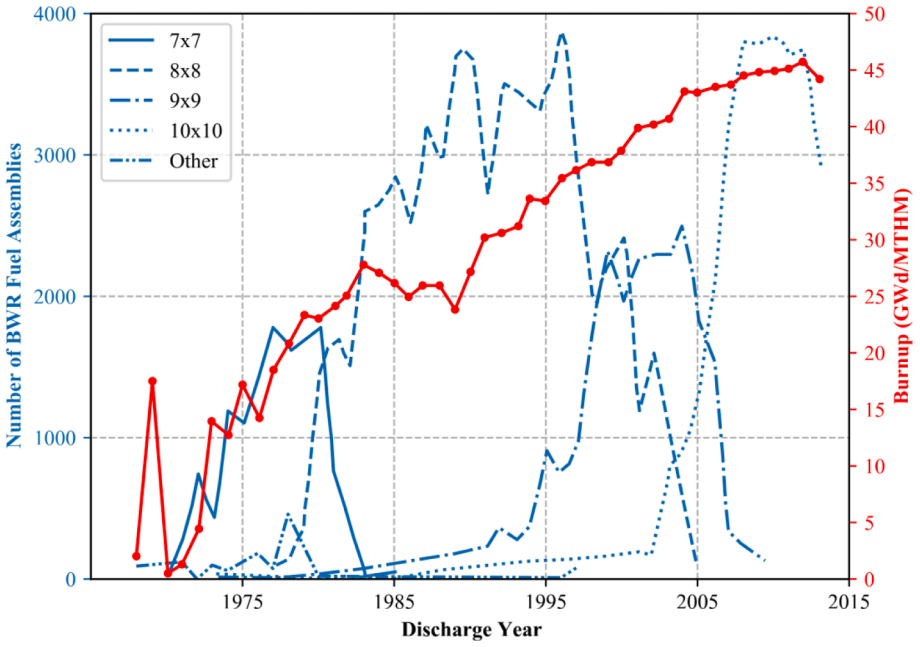

Fig. 2.1. Evolution of the discharge burnup and BWR assembly types in the U.S. from 1968 to 2013 (Hu, et al., 2016).

Table 2.1
Comparison of Selected Element Masses between Reference Study and Scale ORIGEN Results.

Class names in MELCOR	Member of elements	Reference Study (kg) (Carbajo, 1993)	Scale ORIGEN V6.2b (kg)
Noble gasses	Xe, Kr, Rn, He, Ne, Ar, H, N	463.7	446.7
Alkali metal	Cs, Rb, Li, Na, K, Fr, Cu	246.3	256.9
Alkaline metal	Ba, Sr, Be, Mg, Ca, Ra, Es, Fm	207.52	187.19
Halogens	I, Br, F, Cl, At	20.93	17.44
Chalcogens	Te, Se, S, O, Po	40.78	40.99
Platinoids	Ru, Pd, Rh, Ni, Re, Os, Ir, Pt, Au	306.99	296.6
Transition metals	Mo, Tc, Nb, Fe, Cr, Mn, B, Co, Ta, W	350.69	324.98
Tetravalents	Ce, Zr, Th, Np, Ti, Hf, Pa, Pu, C	593.65	554.22
Trivalents	La, *Pm*, Sm, Y, Pr, Nd, Al, Sc, Ac, Eu, Gd, Tb, Dy, Ho, Er, Tm, Yb, Lu, Am, *Cm*, Bk, Cf	571.03	528.0
More volatile main group metal	Cd, Hg, Pb, Zn, As, Sb, Tl, Bi	1.41	1.284
Less volatile main group metals	Sn, Ag, In, Ga, Ge	8.59	8.917

3. ASTEC model of Peach Bottom Unit-2 nuclear power plant

Dimensional data of the core, fuel rods, pressure vessel and volumes of the sections were taken from the document which is prepared by the General Electric Company that includes plant design and operating data for the cycle 1 and 2 (Larsen, 1978). Model definitions, physical modules described in the following sections.

Reactor core and pressure vessel of BWR4 type Peach Bottom Unit-2 nuclear reactor defined under ICARE and CESAR modules of ASTEC. Pressure vessel consist of two structures, which are cylindrical part that holds the core structures and hemispherical volume that represents the lower plenum. Axial meshing starts from the 0.0 m to 4.1191 m elevation level. Fuel channel boxes placed alongside the axial meshing of the

Table 4.1
Design parameters and stationary results of Peach Bottom Unit-2 ASTEC model.

Reference Design Parameters (Larsen, 1978)		ASTEC
Core Power (MW)	3293	3293
Feedwater mass flow rate (kg/s)	1679.68	1673.83
Total mass flow rate (kg/s)	12914.78	12914.89
Core mass flow rate (kg/s)	11336.75	11336.84
Bypass mass flow rate (kg/s)	1578.03	1578.05
Steam mass flow rate (kg/s)	1685.98	1673.83
Steam temperature at dome (K)	559.29	559.38
Core outlet temperature (K)	560.48	559.33
Core inlet temperature (K)	548.53	547.39
Feedwater temperature (K)	464.32	464.32
Dome pressure (MPa)	7.033	7.033
Core outlet pressure (MPa)	7.1564	7.0366
Pressure drop over the core (MPa)	0.152	0.1017
Core inlet pressure (MPa)	7.3084	7.1383
Core exit void fraction	0.65	0.71
Core avg. void fraction	0.304	0.43
RPV water level (m)	14.326	14.278

core domain. Fuel cladding structure placement starts from the 0.0379 m up to 4.1023 m level which encloses the active core material of UO_2. Between 0.0589 m and 3.7169 m axial elevations fuel material was defined. At the same axial level of UO_2, absorber material B_4C and cladding stainless steel around were placed. There are 10 uniformly distributed axial mesh in active fuel domain and 2 additional meshes presents at the top and bottom of it which can be seen in Fig. 5.1. Axial meshes are not equally divided in all levels, in the figure it was only shown for representative purposes.Fig. 2.2.Fig. 2.3.Fig. 2.4.Fig. 2.5. Fig. 4.1.Fig. 4.2.Fig. 4.3.Fig. 4.4.Fig. 4.5.Fig. 4.6.Fig. 4.7.Fig. 4.8. Fig. 4.9.Fig. 4.10.

Reactor vessel internal radius is 3.1875 m and has thickness of 0.1635 m. Inside of the vessel, “downcomer” and “jet” flow channels defined and separated by “jetpump” solid macro structure in order to carry out an external recirculation flow. Reactor core flow inside of the shroud structure divided into 4 channels which are bypass1, bypass2, bypass3 and bypass4 (Fig. 5.1).Fig. 5.2.

Total number of fuel assemblies in the core is 764, their structure type selected as BOX4SIDE rectangular model of ICARE and all assemblies are selected as Type-1 (General Electric 7x7) initial loading. Fuel

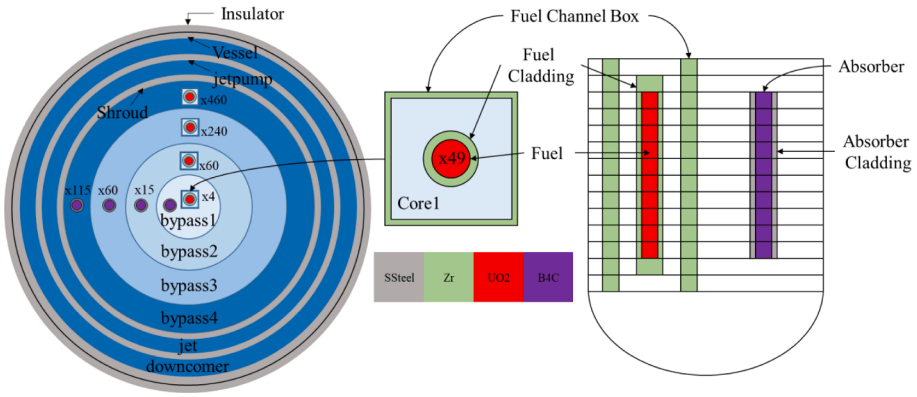

Fig. 2.2. ICARE radial meshes (left) and axial meshes (right) of the core with fuel channel box (BOX4SIDE) and absorber structure equivalents in the each channel.

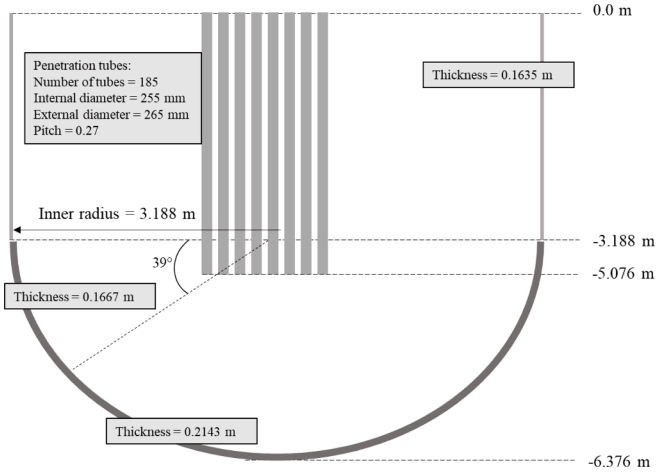

Fig. 2.3. ICARE Lower Plenum elevation points, dimensions and inner structures.

assemblies made of Zr placed inside the core channels as 4, 60, 240 and 460 respectively. Thickness of rectangular macro structure is 2 mm, and have width of the 0.138 m. Number of fuel rods in each fuel assembly is 49 and external diameter of Zr clad structure is 14.3 mm with 0.815 mm thickness. Inside the cladding, diameter of fuel pellet made of UO_2 is 12.37 mm.

Inside the fuel assemblies there are also additional flow channels "core1", "core2", "core3" and "core4" which are responsible of the active core cooling. Therefore, flow channels "bypass1", "bypass2", "bypass3" and "bypass4" that defined inside the "shroud" remains outside of the fuel assembly and they are treated as bypass flow regions. Bypass flow sections have no direct contact with fuel rods unless there is a failure in fuel channel box structures.

Cylindrical control rod structures placed in each bypass channel as 1, 15, 60 and 115 respectively. Stainless steel cladding of control rods has 39.1 mm external diameter. Neutron absorber material B_4C with diameter 32.1 mm placed inside the cladding. During representation of cross-type absorber blades into the cylindrical shape, mass of B_4C and stainless steel preserved, however definition of cylindrical geometry caused under estimation of surface area (Chatelard, et al., 2016).

The lower plenum lies axially below the cylindrical part of the vessel. Domain of the lower plenum lies along the point 6.376 m to 0.0 m. The cylindrical portion of the lower plenum begins at 0.0 m in height and extends to the 3.188 m point. Below this point the hemispherical portion of the lower plenum stays. The inner radius of the cylindrical part is 3.1877 m and the wall thickness is 163.5 mm. The wall thickness of the hemispherical part is 166.7 mm up to the 39th degree and 214.3 mm thereafter (Fig. 2.2). The number of steel pipes is 185, the outer diameter of the pipes is 265 mm and the thickness is 5 mm.

Definition of the support plate structure can be found the PWR type power plant reference input decks in ASTEC. However, definition of

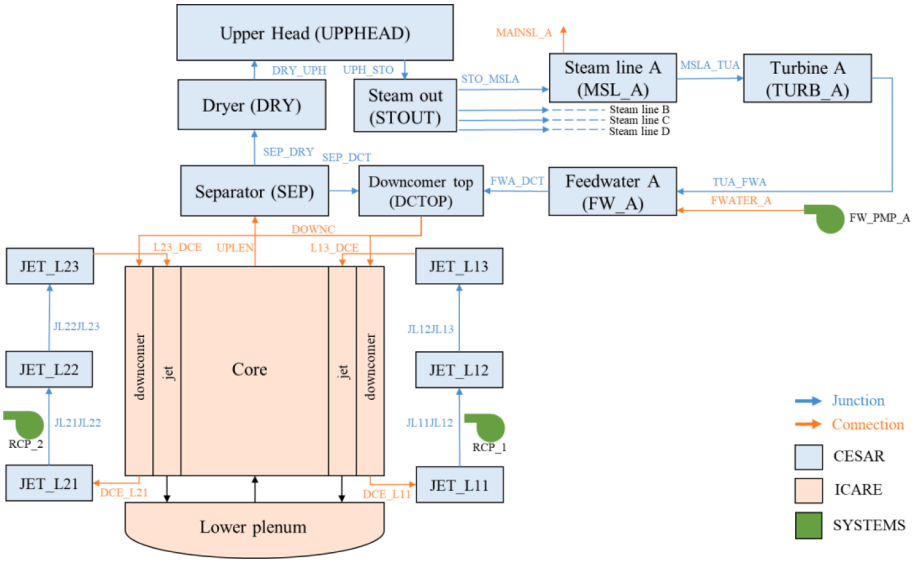

Fig. 2.4. CESAR volumes, junctions, ICARE core domain and their connections of RPV of Peach Bottom Unit-2 Model.

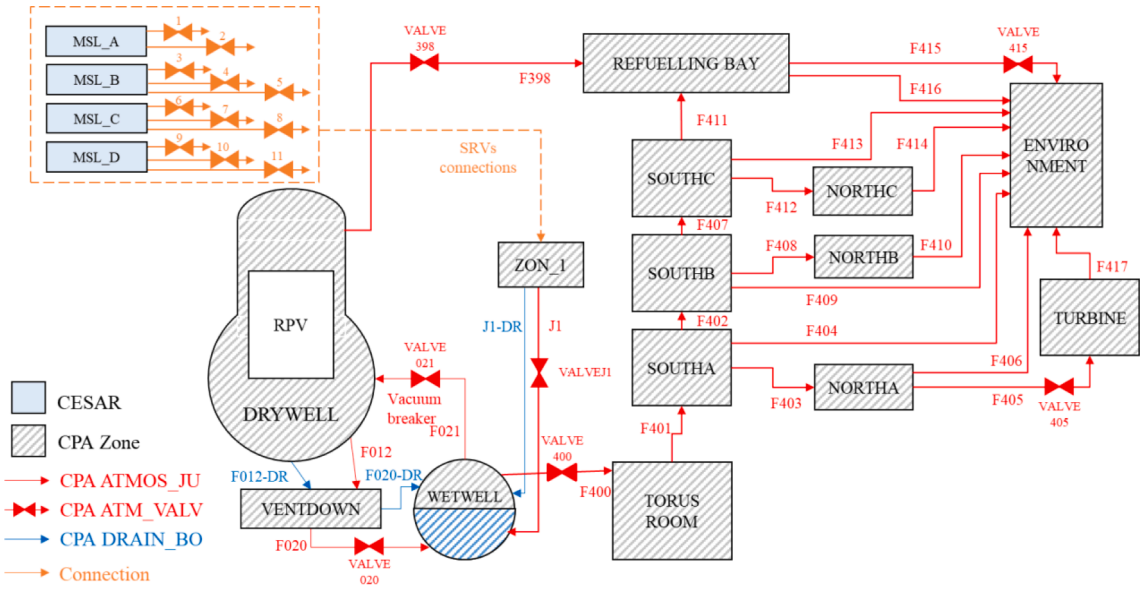

Fig. 2.5. CPA zones that represents Primary Containment Vessel and reactor building sections of ASTEC model of Peach Bottom Unit-2 Reactor.

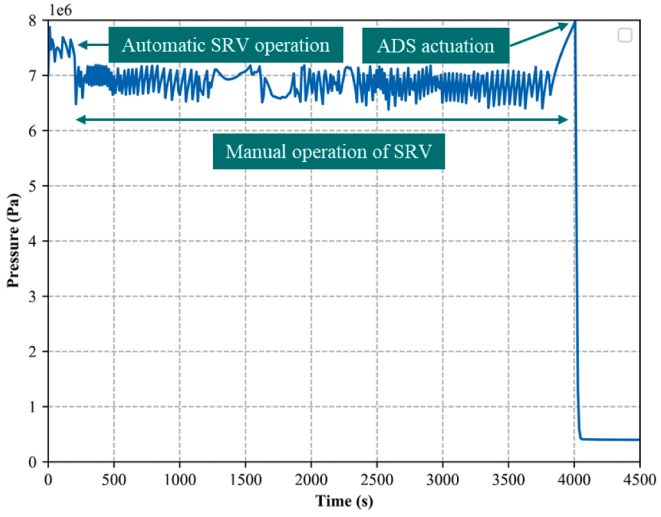

Fig. 4.1. Vessel pressure during automatic SRV-1 and manual SRV operation.

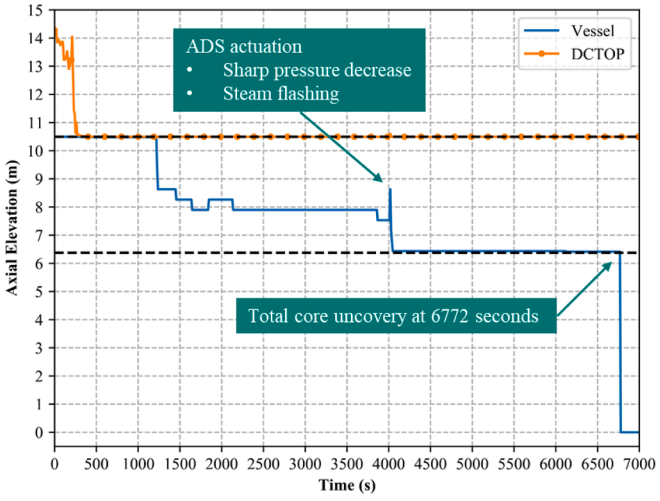

Fig. 4.2. Water level inside the vessel (ICARE domain) and top of the downcomer (DCTOP).

canisters in BWR input deck creates non-concentric sub-channels separated by solid structure. Description of the support plates not included based on the recommendations for definition of plate structure for non-concentric sub-channels.

Recirculation lines of BWR type reactors modeled with CESAR volumes (3 volumes for each recirculation line) and connections between them. After the "downcomer" channel, the connections take water from the bottom of the channel and direct it to the first volumes of the recirculation lines (JET_L11 and JET_L21). The water is directed through the second volumes (JET_L12 and JET_L22) with the help of recirculation pumps. Then, the flow path of the recirculation pipes ended with connections that connect the CESAR volumes (JET_L13 and JET_L23) and the ICARE channel "jet". The jet channel directs water to the lower plenum and then to the core region. The water is heated to saturation temperature and reaches the SEP volume of CESAR. The liquid water is separated from the SEP volume into the DCTOP volume and then the water enters the downcomer channel to recirculate again.

The PCV sections and the reactor building volume, their connections and failure modes were constructed using the CPA module of ASTEC, taking into account the MELCOR design of the previous study (Carbajo, 1993). Drywell, wetwell and vent down zone with their connections each other forms the PCV structure of the reactor. The definition of the vent pipe in ASTEC only possible if it is located between two CPA zones. For this reason, the definition of the ZON_1 zone provides a necessary zone for the connection of the vent pipe, which submerges into the wetwell pool. The F021 vacuum breaker connection ensures that the pressure level in wetwell zone does not exceed the pressure level in drywell zone by opening and allowing a mechanical equilibrium between the two zones. The F398 connection between the drywell and the refueling bay and the F400 connection between the wetwell and the torus compartment simulate the containment failure paths. The first failure mode, rupture of the wetwell compartment defined for the case when the pressure in wetwell reaches 1.2 MPa. The second mode, the F398 connection, simulates the rupture of the flange of the drywell head when the temperature rises to 644 K and the pressure in the drywell reaches to the 0.565 MPa. The high temperature in the drywell disturbs the flange structure and destroys the elasticity of the material, and the high pressure creates paths through the refueling zone. The size of the crack in the flange depends on the pressure in the drywell and changes linearly between 0.565 MPa (0.0 m^2) and 1.378 MPa (0.04 m^2).

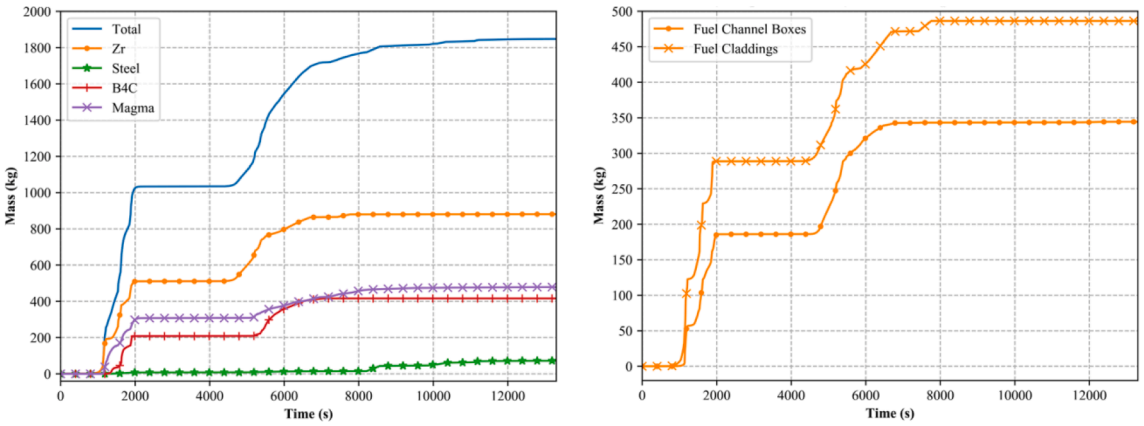

Fig. 4.3. Generated hydrogen mass caused by the oxidation of the structures in the core (left) and Zr structures fuel channel boxes and fuel claddings (right).

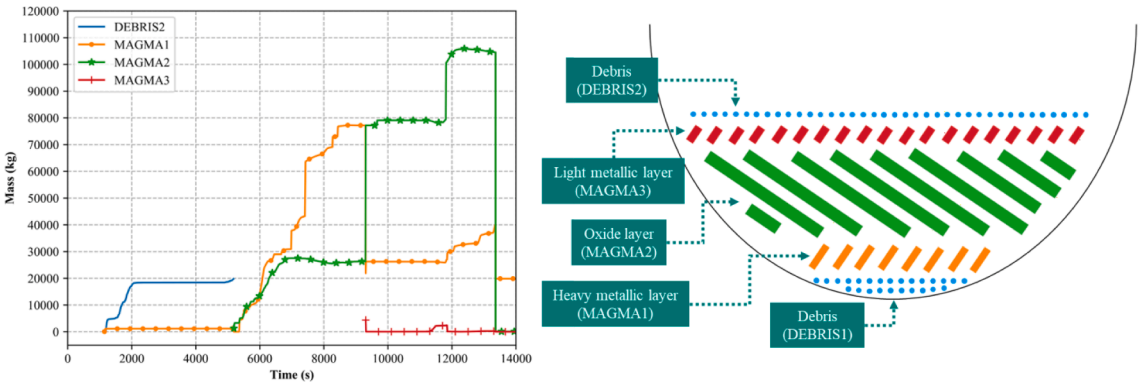

Fig. 4.4. Corium mass in lower plenum (left) and ASTEC typical debris configuration in lower plenum (right).

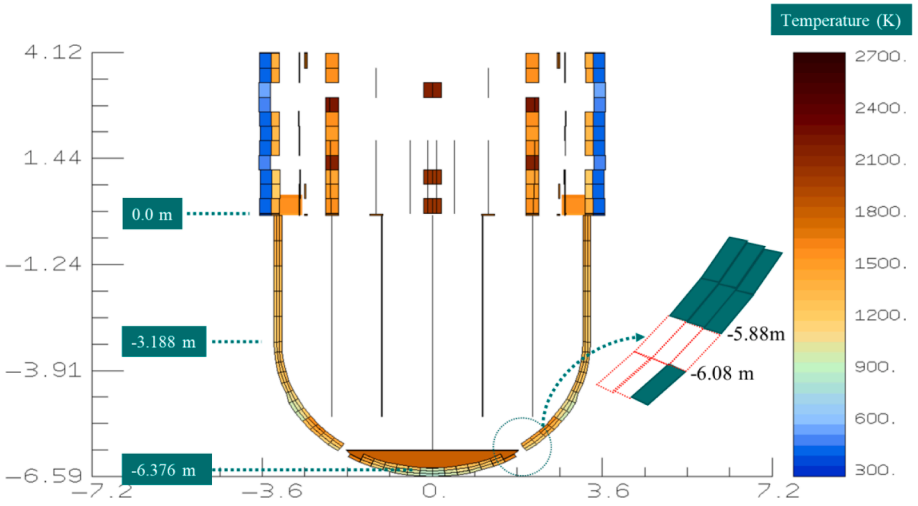

Fig. 4.5. Degradation level and temperature levels on the point of lower head failure.

Connections of the SRVs from steam line volumes of the CESAR through to the wetwell zone which hosts the suppression pool can be seen in Fig. 2.4. Since the opening and closing pressures of the SRVs are different from each other four steam line model as it is in the design of the reactor was introduced to the ASTEC model. Automatic Depressurization System (ADS) consist of operation of the SRV number 1, 2, 3, 5 and 6.

Definition of the single cavity in the ASTEC model was made in the drywell zone. Geometrical definition of the cavity as follows; basemat thickness is 1.524 m, cavity height where molten material collected is set 2.457 m, cavity radius is 6.48 m and thickness of the lateral walls is 0.52 m. Concrete material composition fractions in the cavity 0.338 CaO, 0.358 SiO_2, 0.072 H_2O, 0.206 CO_2, Al_2O_3 0.009 and Fe 0.017 and ablation temperature of the concrete is set to 1503 K. Single cavity model of the previous study (Carbajo, 1993) was referenced for the cavity model of the ASTEC.

ASTEC FP_HEAT rubric, which includes isotope fractions as well, is responsible for the decay heat production. Calculation of the fuel

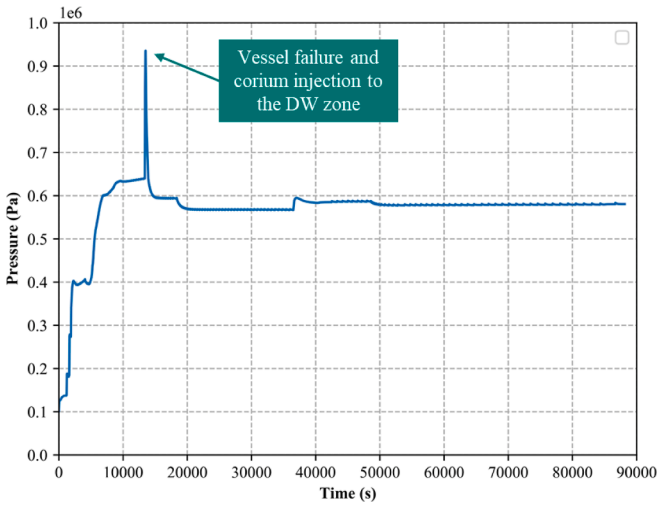

Fig. 4.6. Drywell Zone pressure up to end of the ASTEC transient simulation.

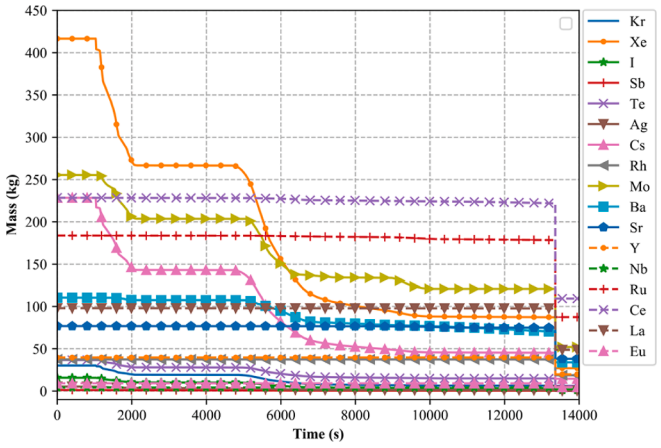

Fig. 4.7. Fission products in the core domain.

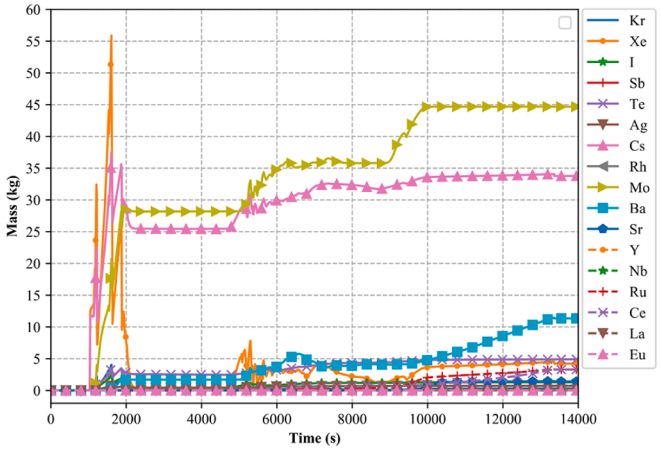

Fig. 4.8. Fission products in the CESAR Volumes.

inventory, in order to make better source term estimation, was performed by using Scale ORIGEN code which detailed explanations can be found in the section 3.

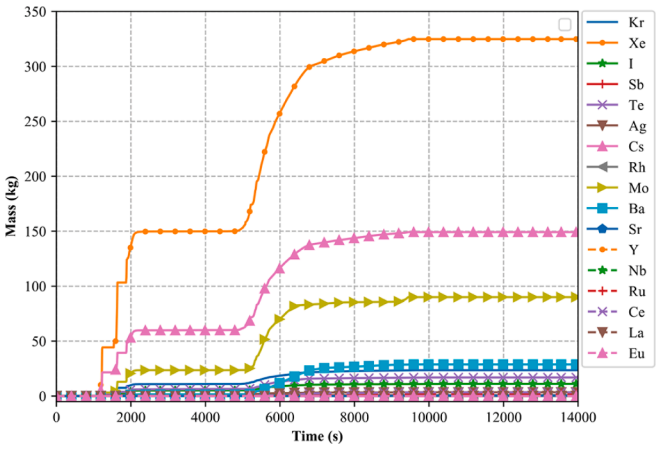

Fig. 4.9. Fission products in the CPA Zones.

3.1. Considered physical phenomena in ASTEC model

Modeling of the Peach Bottom Unit-2 in ASTEC requires definition of physical models which are responsible for heat transfer, chemical interactions, failure criteria and material movement. Selected models and their definitions for the related domain explained in this chapter.

3.1.1. Heat transfer models

In order to define conductive heat transfer in macro components or between macro components automatic definition of CONDAUTO was used. Module RADR definition was also made for radiative heat transfer between structures in the core up to cavity occurs. Described RADASSEM module takes action to calculate radiative heat transfer after cavities appear. New implementation of the radiative heat transfer capabilities for the fuel channel boxes in BWRs also was taken into account thanks to RADASSEM module. In addition, heat transfer mechanism between fluid and macro structures was build by CONVAUTO option. In order to define in mesh heat transfer models, which includes molten pool heat transfers between its meshes, POOL option was enabled. In POOL option MAYINGER model (default) was selected which assumes homogeneous temperature in corium pool and uses specific correlation to find characteristic velocity of the pool in order to get mixing conductivity.

3.1.2. Chemical reactions and interactions

Oxidation of zirconium with steam was provided by structure ZROX. Cladding of fuel rods, canisters of fuel bundles and spacer grids were included in the ZROX and BEST-FIT option was selected. In order to deal with steel oxidation by steam FEOX structure was defined for external face of absorber rod cladding and internal faces of the shroud and vessel structures. Steel oxidation kinetic option was selected default value MATPRO that considers the correlation of J.WHITE (White, 1967) studied on type 304 stainless steel. Module BCOX structure models the boron carbide oxidation by steam. Default option for oxidation kinetic BEST-FIT considered in range of experimental studies done with VERDI facility and BOX rig experiments in frame of COLOSS project (Adroguer, et al., 2003). Eutectic interaction between stainless steel and boron carbide was activated by BSCC structure. Melting point of boron carbide is around 2350 °C and for stainless steel is around 1450 °C. Due to eutectic interaction between boron carbide and stainless steel, formation of the liquefied stainless-steel layer can be observed around 1200 °C which is 200 °C lower than melting point of stainless steel (Nagase, et al., 1997). Modeling of the boron carbide and stainless-steel interaction by BCCS structure of ASTEC is based on the PWR type (rod like) cylindrical boron carbide rods. Implementation of this module is adaptation of blade structure as a cylindrical structure. Dissolution of UO_2 and ZrO_2 by liquid zircaloy is also considered chemical reaction during severe

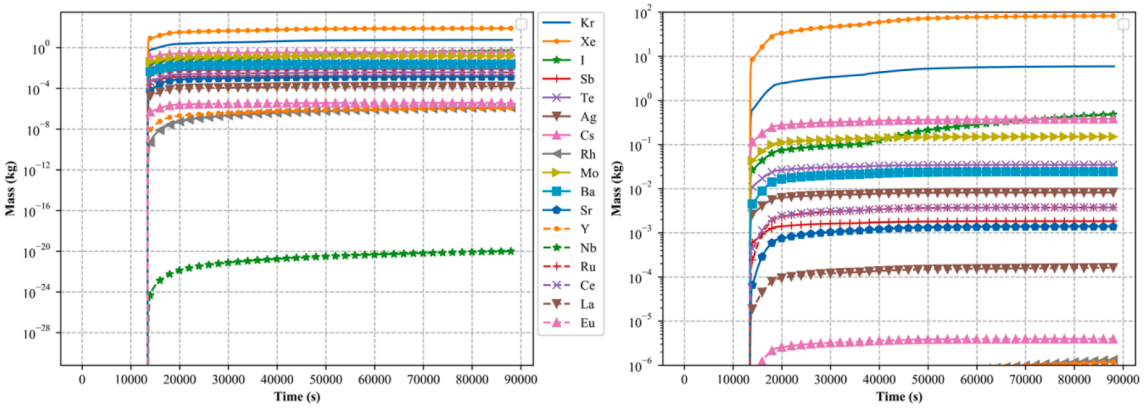

Fig. 4.10. Fission products release to the environment cumulatively.

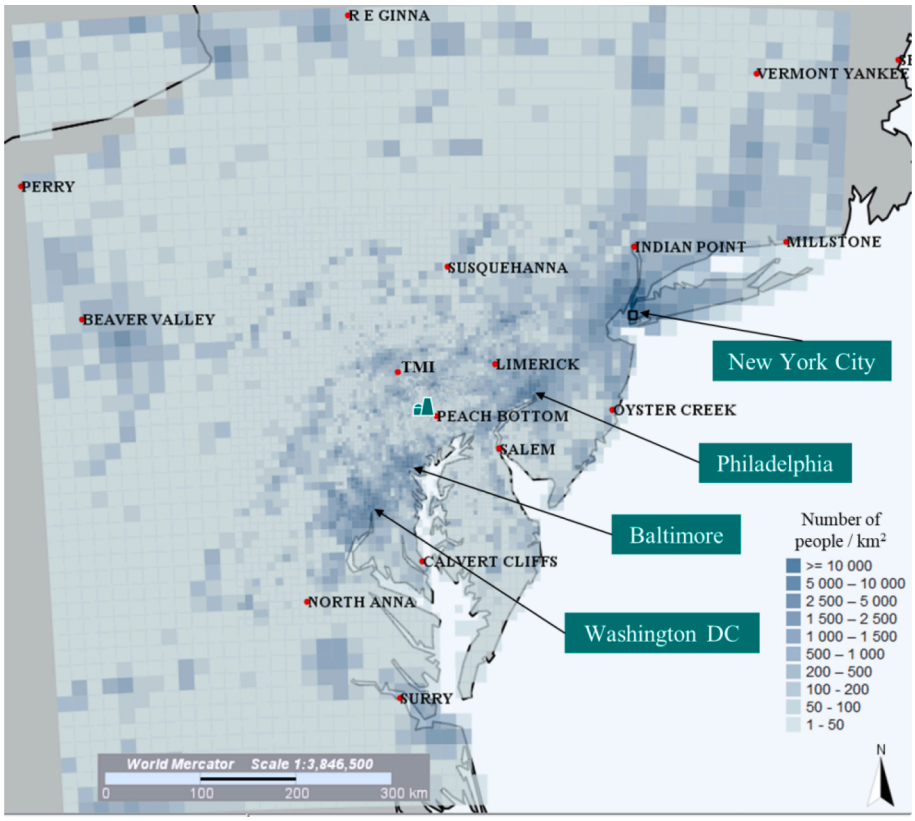

Fig. 5.1. Mesh grid in 400 km range around the Peach Bottom NPP site and population distribution over grid.

accident conditions. Structure UZRL activated to ensure interaction take place between UO2 fuel material and zircaloy cladding. Chemical interactions associated with magma component is structured by the UZOXMAG option.

3.1.3. Mechanical behavior

Mechanical behavior of the UO_2 fuel material enclosed with Zircaloy cladding structures are first safety barrier for radioactive material. Their integrity and related parameters defined under mechanical behavior options of the code.

CREE structure was defined for creep behavior of the Zircaloy cladding and the model is only available for Zr layer. All cladding groups in each channel included in the structure with the following options. Best estimate physical model for burst occurrence EDGAR option was selected. Gap pressure between fuel rod and cladding was set to 30 bar and EPMX hoop creep and CRAC burst criterion parameters selected as 0.25 and 0.5 respectively as indicated as recommended values for reactor applications.

Integrity criteria of the fuel, cladding and canister structures was defined using by INTE structure. For fuel macro structures, condition would set to DISLOCAT if the temperature was greater than 2500 K. DISLOCAT status of the material starts degradation of the macro structure. It is not mandatory to contain molten material for degradation state but can contain MIXTU structure, which is not explicitly user defined layer. DISLOCAT state also allows fission product release and double sized oxidation. Cladding INTE structure conditions was set to two branches. If the temperature reached to 2500 K status would set DISLOCAT. In addition, if temperature level exceeded 2300 K and thickness of material layer decreased to 250 μm, status of the cladding would set DISLOCAT as well. Integrity criteria of the canister structures includes

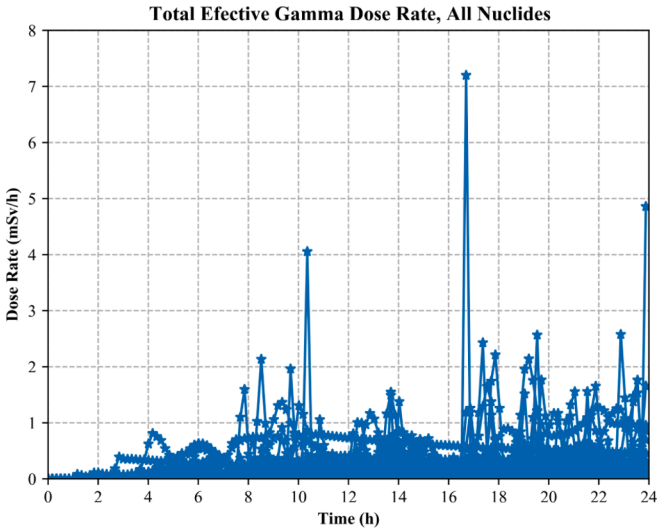

Fig. 5.2. Total effective gamma dose rates of one day simulations for one year (2021) among the interested meshes.

the condition of temperature which greater temperature level than 2500 K leads to DISLOCAT status.

DECAUTO automatic model definition was made to provide material movement inside mesh. From one set of structure like rod can be transferred to another set such as grid in the same mesh domain. In order to deal with melt corium movement in core region MOVEMAG option with LEAK setting enabled. Setting LEAK provides material transition from core region to lower plenum domain.

Integrity lost criteria for the lower plenum meshes are adopted from the reference study (Carbajo, 1993) as when the temperature of the mesh reaches 1723 K rupture option in the LOWERPLE structure activates and mesh disappears.

3.1.4. Physical phenomena in lower plenum

Corium melt movement started with MOVEMAG structure and LEAK setting provides a breach from core to lower plenum and other end of the breach was defined with SLUMP structure. User needs to define SLUMP structure in case of lower plenum domain exist and corium melt movement transfers to lower plenum. FRAGLOWE option is enabled to activate corium fragmentation in lower plenum when the melt is contacted with water in lower plenum and it undergoes the fragmentation. Material separation in lower plenum, when corium is collected in and metallic composition starts to be collected at the top of the heavier oxide layer, provided by SEPALOWE structure. Movement of the debris bed particles which are located above the liquid corium pool defined with MOVELOWE structure. Debris particles can penetrate and sink into corium pool beneath.

3.2. Boundary conditions

Water injection to the vessel described with connections named FWATER and, as a boundary condition, 191.17 °C water was fed at a rate of 419.92 kg/s rate to each feed water volume in CESAR. Pressure boundary conditions were described for the volumes of steam pipe in CESAR for steam extraction. The pressure parameter was set to 7.0268 MPa to keep pace with the design pressure of the vessel dome during steady state calculations. Thermal heat exchange was introduced with the boundary condition HEAT from the volumes CESAR to the CPA zone drywell in the PCV domain. In order to allow the molten material to transfer from the vessel to the containment and cavity, the boundary condition VESPOUR was described. The definition of the cavity was already done in drywell zone in CPA. However, to impose direct heating of the containment, the boundary conditions DCH and MCCI were activated.

4. Analysis of the ST-SBO for Peach Bottom Unit-2

Steady state results and established transient scenario and ASTEC predictions presented in this section. CESAR, ICARE, CPA, ISODOP, SOPHAEROS, RCSMESH, MEDICIS, RUPUICUV, CORIUM and DOSE modules activated for the calculations. Execution of ST-SBO scenario resulted around 9 h CPU time with ASTEC V2.2 Revision 6790 M developer version, which is compiled with GCC 12.2.0 package in Windows.

4.1. Stationary plant conditions at nominal power

Calculation executed for 500 s and results are presented in Table 4.1. Discrepancy between inlet pressure resulted higher amount of steam production in the core and larger void fraction in general. Since the basic channel application was introduced without jet pump, increase in the pressure was not observed.

4.2. Short term Station Black-Out accident

Decision of the severe accident scenario was made based on the previous safety assessment studies on BWRs. Even though the referenced study with MELCOR (Carbajo, 1993) considers the SBO accident transient, it must be emphasized that the choice of severe accident scenario must be based on a solid foundation.

Based on previous safety assessments (Kolaczkowski, et al., 1989) the loss of offsite power (LOSP) scenario with diesel generator failure and battery depletion was found to have the greatest impact on the core damage frequency of the Peach Bottom Unit-2. This work was also part of the complementary study of severe accident risk analysis of five nuclear power plants that included Peach Bottom Unit-2 (U.S. Nuclear Regulatory Commission, 1990), and as part of that work, SBO accidents were again found to have the highest core damage frequencies among the estimated transients. Another study (Leonard, et al., 2007) also showed that Short-Term Station Blackout (ST-SBO) with a stuck open relief valve is one of the major contributor to the core damage frequency.

Another important point: the calculation time of the SBO scenarios without safety systems was the fastest compared to the other estimated transients, which contributes to fast simulation runs and easier examination of the results. Based on the studies and conclusions, it was decided to follow the same transient with the reference MELCOR work.

Initial event was loss of offsite power following with all diesel generators failure and battery depletion. Reactor scram was initiated at time $t = 0$ with containment isolation which is main steam line and feedwater line closure. Operation of the SRV-1 for 200 s was assumed which corresponds the time period until operator actions takes place to depressurize the reactor. After that, manual operation of the one safety valve continued between 6.49 MPa and 7.18 MPa. Operation was carried out until water level in core reaches one third of the core level and following ADS operation initiated. Calculation executed until the basemat in the cavity domain ruptures.

4.2.1. Main results of ST-SBO transient

Estimated events during calculations are presented in order Table 4.2. Each saved sequence represent steps of the propagation of the severe accident starting from the failure of the fuel cladding structure up to rupture of the basemat structure in the cavity.Table 4.3.

After the plant is shut down, the decay heat increases the temperature and pressure inside the vessel. The pressure inside the vessel increases to the opening set point of SRV-1, which has the lowest set point between SRVs, and its automatic operation maintains the pressure between set points until manual operation begins. After 200 s, the operation of one SRV between the 6.49 MPa and 7.18 MPa pressure setpoints

Table 4.2
Sequence of events Peach Bottom Unit-2 ASTEC Model ST-SBO Scenario.

Sequence of Events	Time (s)
SRV-1 starts operation	0
SRV-1 stops operation, Manual operation of a SRV starts	200
First cladding creep rupture, start of the fission product release	1037
First material slump in lower plenum	1142
First slump of corium with fission products in lower plenum	1158
First appearance of a cavity in core	1167
Manual operation of a SRV stops, ADS actuates	3867
First total core uncovery	6772
Lower head vessel failure	13,361
PCV head flange failure	13,415
Basemat rupture	88,142

Table 4.3
Element mass fractions released into the environment.

Element	MELCOR (Carbajo, 1993)	ASTEC
Xe, Kr	0.06	0.198
I	0.0075	0.0308
Cs	0.0097	0.0017
Te	0.0066	9.51E-4
Sr	5.0E-4	1.797E-5
Ba	0.0005	2.2E-4
Ru	3.0E-8	2.05E-5
La	4.0E-7	1.65E-6
Ce	1.0E-7	1.66E-5

continued to depressurize the system, corresponding to the manual action of the operators. Manual operation of the SRV continued until initialization of ADS. At 3867 s, the water level in the core reached one-third of the core level and this triggered the ADS operation. Thus, the triggering of the 5 SRVs resulted in a sudden pressure drop in the vessel (Fig. 4.1). The estimate of ADS triggering after manual actuation of an SRV in the reference study was 3983 s, which is close to the MELCOR and ASTEC results related to SRV operations.

Depressurizing the core by removing steam from the vessel results in a loss of water mass and a drop in the water level in the vessel. As can be seen in Fig. 4.2, the water level is shown in separate domains. Core domain where fuel assemblies were inserted is shown with the name "Vessel" and the water supply to the core, at the top of the downcomer volume "DCTOP". The loss of water mass and the drop in the water level starts at the beginning with the steam extraction by the automatic and manual operation of the SRVs. After the water in the DCTOP volume is depleted, the level in the active core region begins to drop. Activation of the ADS at time 3867 s results in a sudden drop in pressure and a flash of steam causing a sudden jump in the water level in the core. The complete discovery of the core is recorded at 6772 s, which can be seen in Fig. 4.2, After the water level reaches to below lowest axial mesh in the core domain, the water level record drops to zero because the lower plenum representation in ASTEC consists of one mesh and the construction of the average water level was not considered. The reference study (Carbajo, 1993) does not specifically mention the total water depletion including the water level in the lower plenum and the time of core uncovery.

Hydrogen production caused by oxidation of materials in the core is one of the driving mechanisms of core degradation, as this exothermic reaction causes additional energy release in the core. The removal of steam by opening the SRVs and the pressure drop create more steam and a high temperature steam environment that further promotes the oxidation reaction. In Fig. 4.3, the hydrogen mass produced by the oxidation of Zr, stainless steel, boron carbide, and magma structures are shown separately on the left and the Zr structures of the fuel channel boxes and fuel claddings are shown separately on the right up to the time of the bottom head failure. Since the rectangular fuel channel boxes, which are BWR-specific structures, are also made of Zircaloy material, it is important to emphasize whether or not their contribution to hydrogen production is comparable to that of the fuel claddings. Hydrogen production is an indicator of the level of oxidation reaction of the material, which indicates the potential of energy release in case of an exothermic oxidation reaction. The results show that the level of hydrogen production mass for fuel channel boxes is not far from the fuel claddings. Their contribution to the total hydrogen production of 1847.6 kg accounts for half of the mass produced.

Investigation of the ST-SBO accident scenario in the reference study (Carbajo, 1993) consist of two calculation approaches which MELCOR and MELCOR/CORBH. In order to take into account debris quenching with water in lower plenum MELCOR with CORBH package was used. Standalone MELCOR calculation did not include debris quenching and high temperature debris particles directly heated the lower plenum structure. In addition, standalone MELCOR uses multi-node cavity and MELCOR/CORBH deals with only single node cavity which is suited for ASTEC as well. The estimated hydrogen production for the stand-alone MELCOR case is 500 kg and for MELCOR/CORBH is 600 kg, which is far below the ASTEC prediction.

The accumulation of the corium, which is called magma structure in ASTEC terminology, in the lower plenum is shown in Fig. 4.4. It can be seen that mass transition between the heavy, light and oxide layers of the magma and their construction beginning of the corium buildup. At time 13,361 s, failure of the lower head vessel occurs and most of the molten material is ejected from the lower head into the cavity. The total mass of corium ejected from the vessel is predicted to be 152.34 tons. As can be seen on the left in Fig. 4.4, the MAGMA1 heavy metal layer is not completely ejected after the vessel failure, there is still about 20 tons of material in the lower plenum. The amount of failure in the meshes of the lower plenum and the degree of degradation of the core domain (ICARE) at the time of failure of the lower head can also be seen in Fig. 4.5.

The time for lower head failure estimated in the reference study (Carbajo, 1993) for the MELCOR case is 9760 s, considering only penetration failures. In the MELCOR/CORBH case, penetration failure was observed in 17,128 s and complete lower head failure in approximately 28,000 s. The stand-alone MELCOR calculation did not estimate the total lower head failure and showed an early penetration failure due to the excess heat of the debris being directly transferred to the lower head wall. In contrast, the CORBH package accounts for the quenching of the debris and the amount of excess heat removed by the water intake in the lower plenum, resulting in later failure. The mass ejected from the lower head is approximately 180 tons for the MELCOR standalone case and 279.52 tons for the MELCOR/CORBH package. A larger amount of material is expected to be ejected in the case of the CORBH package because a complete failure of the lower head is observed. The comparison between the previous study and the ASTEC results shows major differences. Definition of the lower head structures in the ASTEC model consists of cylindrical structures that do not fully correspond to the complex framework of the lower head of the BWR. For this reason, the MELCOR model considers a larger material definition and the consideration of penetrating tubes in the lower plenum with a larger mass. After the total failure of the lower head for MELCOR/CORBH and only the failure of the penetration tubes for the standalone case, a larger mass was ejected from the lower plenum. In addition, a larger thermal mass extends the period of lower plenum failure by increasing the total heat capacity of the structural system in the lower plenum.

After the failure of the vessel, the accident transient continues in the PCV domain which deals with phenomena outside the vessel. Extracted steam and fission products from the core inserted in the wetwell zone through vent pipe connection that allow the suppression pool scrubbing during the SRV and ADS operations. Condensation of the steam retention of the fission products with carrier gasses takes place in the suppression pool and excess mass transfers to the air atmosphere of the wetwell zone and drywell zone. During the ST-SBO scenario high temperature and pressure build up in the drywell activated the failure mode for the head flange failures in the drywell. In Fig. 4.6, it can be seen that pressure rises resulting action of the SRV and ADS operation and vessel

failure causes sudden increase in the pressure in the drywell since the cavity is defined in the drywell zone. Activated head flange failure mode opens the Valve-398 and allows the fission products to reach environment at 13,415 s. Pressure level circulates around 600 kPa in Fig. 4.6 since the opening on the flange is dependent on the pressure in drywell zone and opening and closure of the connection causes this behavior.

MELCOR/CORBH calculation was terminated before the containment failure, and only the stand-alone MELCOR calculation was continued in the previous study. The head flange failure in the drywell zone was also the driving mode for the containment failure in the MELCOR study. Head flange failure was observed at 25,515 s, which is larger than ASTEC prediction. Standalone MELCOR simulation prediction for the amount of mass ejected from the lower plenum is comparable to the ASTEC prediction, but the MELCOR simulation only predicts penetration failure without failure of the entire lower head, and the pressure accumulation is slower than the ASTEC model. For this reason, the accumulation of temperature and pressure in the MELCOR model takes longer than in the ASTEC model and the MELCOR estimation of PCV failure is in later stages than ASTEC.

Fission product inventory in the core until vessel failure is shown in Fig. 4.7. After the loss of cladding integrity, the fission products begin to move from outside the fuel domain. The production of steam and removal by the SRVs transports the fission products along the path. The sudden drop in fission product masses in Fig. 4.7 at time 13,361 s corresponds to the failure of the lower head. After that point, the calculation of the ICARE and CESAR modules is stopped and the last stored parameters remain in the database.

Operation of the SRV steam extraction and fission product transportation also can be tracked in the Fig. 4.8. Large jumps at the beginning caused by the manual operation of the SRVs and after ADS actuation at the 3867 s there is a slight increase in the fission product masses.

After the CESAR volumes, which SRV connections were made, CPA zones simulates containment for the ex-vessel phenomena and final barrier between fission products and environment.

The accumulation of fission products in the environment is shown in Fig. 4.10. The logarithmic scale was used to show the fission product masses in one place because the quantities on the y-axis are widely separated. The low retention rate of the noble gasses results in a significant amount of them being released into the atmosphere. At the end of the calculation, the total activity released to the atmosphere was recorded as 1.836E18 Bq. The comparison between the MELCOR reference study and the ASTEC model in terms of elemental fractions released to the environment is shown in Table 4.3. The magnitude of the two studies shows that the results are comparable and the simulation transient followed in the same direction.

In order to make a conclusion about released fission products to the environment in terms of public safety and to understand possible consequences caused by them further analysis needs to be performed. In order to achieve that JRODOS implemented to continue complementary work.

5. Statistical analysis of the fission products dispersion and worst case scenario approach with JRODOS

Assessment of the fission product release to the environment is the next step of the calculation and it was carried out with Java based Real-time Online Decision Support code (JRODOS) (Ievdin, et al., 2010). The RODOS code was developed to meet the needs of decision makers in nuclear accidents. The main objective was to estimate the doses and the effects of radiological dispersion on the environment and the population, taking into account the geographical shape of the area, the distribution of the population, and the weather conditions. The development of models and better estimation of radiological dispersion assists decision makers in conducting analyzes in possible accident scenarios and in improving emergency management guidelines.

In order to understand the possible consequences of ST-SBO accident in Peach Bottom Unit-2, masses of the fission products that estimated in environmental release by ASTEC, converted into JRODOS source term information. Point of release was selected as actual geographical location of the Peach Bottom NPP in the databank of the JRODOS and meshed grid was constructed around it within 400 km radius (Fig. 5.1). ASTEC simulation showed that release duration of the fission products to the environment was about 20.75 h and this duration divided into 30 min time steps. Amount of released fission products described as source terms for each time interval.

The radiological dispersion analysis does not include a detailed study of the source term release consequences in terms of public safety. The main objective of the following part of the study is to examine the statistical analysis on the considered region over a time period in order to understand potential consequences based on worst-case approach.

The selection of analysis for each day for JRODOS simulations were performed for 24 h. In order to be able to perform a statistical analysis for one year on the selected area with a personal computer in a reasonable time the simulations were performed for one day.

As can be seen in Fig. 5.1, the population is widely dispersed along the east coast of the United States. Examining each residential area through the grid is difficult to evaluate and draw some conclusions. For this reason, only certain meshes that have higher population densities than others in the region were selected as points of interest. Selected meshes on the map as follows; mesh number 5554, 5606, 5658, 5607 for the New York City, mesh 3209, 3240 and 3241 for the Philadelphia, mesh 2064 and 2065 for the Washington DC, mesh 2594 for the Baltimore. Average population density in the New York City is around 17,000 people/km^2, Philadelphia has around 8000 people/km^2, Washington DC and Baltimore City have around 5000 people/km^2 for their corresponding meshes.

The simulation of the 24 h requires the weather data from initial time to the end of the simulation and any recorded or user defined weather definition could be described in the JRODOS. An investigation of the weather conditions that could potentially produce the highest dose rate in the selected meshes was performed to pursue the worst-case approach. A weather database for the year 2021 was selected and a simulation was run for each day from January 1, 2021 to January 1, 2022, without considering early countermeasures. The start time for the simulation was randomly selected for each day.

Maximum recorded total effective gamma dose rates on each day in 2021 between the interested mesh points are shown in Fig. 5.2. Maximum dose rate on each day was recorded 178 times in New York City, 98 times in Philadelphia, 6 times in Washington DC, and 48 times in Baltimore. The total number is not equal to 365 because on some days the weather conditions favored the selected mesh points as they did not receive fission products and for this reason no dose rate was recorded. Of all the days recorded, the highest dose rate was recorded in mesh number 2594, corresponding to Baltimore City, at 7.2 mSv/h when the release of fission products begins at 10:33 am on February 12, 2021.

A single simulation was performed to examine the example representing the highest total effective gamma dose rate in the statistical analysis. The calculation was started at 10:33 a.m. on February 12, 2021, and ended 24 h later, excluding early countermeasures. As can be seen in Fig. 5.3, the affected area of Baltimore City receives no dose during the first 12 h because of wind direction carries the fission products to the west. However, the wind direction changes and the results after 18 and 24 h show that the propagation of the dose rate to the east decreases and the cloud covers Baltimore City, resulting in a total effective gamma dose rate of 7.2 mSv/h in mesh 2594, as shown in the statistical results (Fig. 5.2). The clouds cover not only the Baltimore area but also other counties to the west of the Peach Bottom NPP. After the change of wind direction, the Washington DC area also receives a total effective gamma dose rate of about 2 mSv/h in this case.

The limit on total effective dose equivalent for individuals of the public and for radiation workers in a year has been set by the United

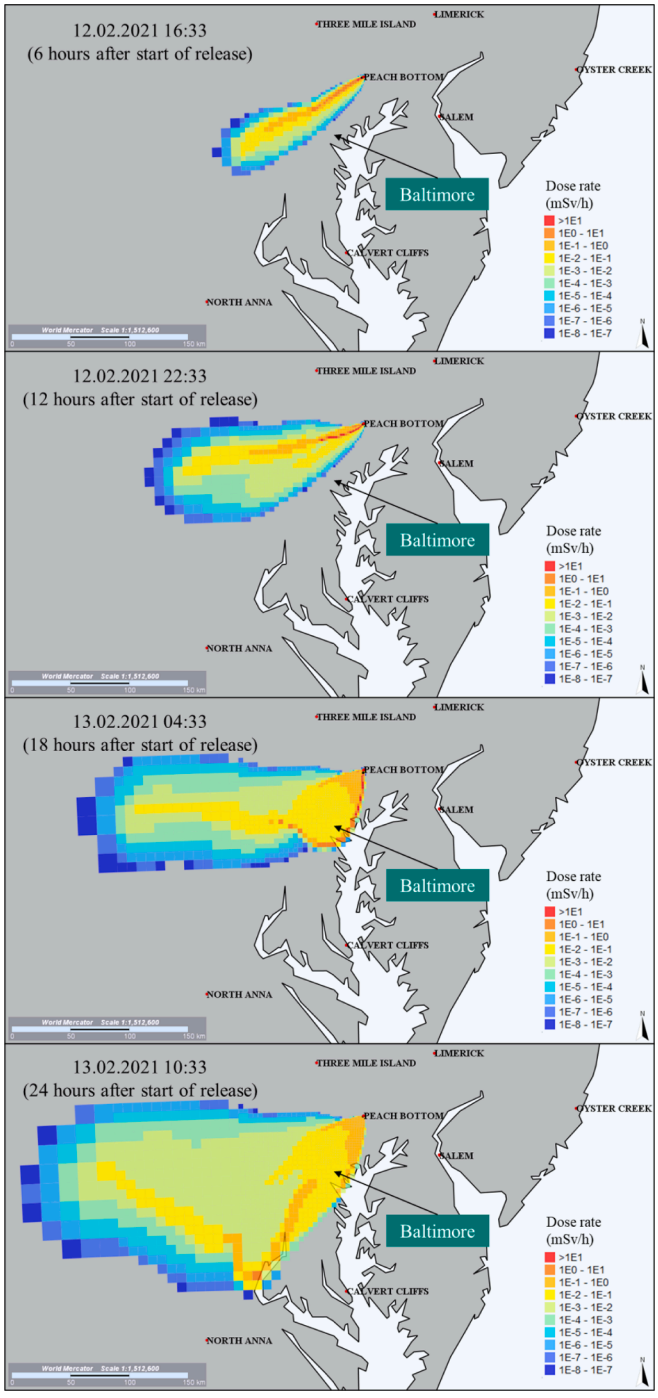

Fig. 5.3. Total effective gamma dose rate map for 6, 12, 18 and 24 h after fission products release resulted by ST-SBO accident in Peach Bottom Unit-2 NPP within the constructed domain in JRODOS starting from 12th of February 2021 at 10:33.

States Nuclear Regulatory Commission (USNRC) at 1 mSv and 5 mSv, respectively (U.S. Nuclear Regulatory Commission, 1991). The comparison between the highest recorded dose rate and the annual limits shows that the dose rate is high enough to exceed the limits, regardless of whether the persons are members of the public or radiation workers. This result is not unique to Mesh 2954, which corresponds to Baltimore City. There are also regions that were not considered in the statistical analysis where dose rates are as high as in the affected meshes. However, the selection of points took into account that cities with larger populations can potentially have more severe consequences.

6. Conclusion and outlook

An overall study of a severe accident was performed, starting with fuel inventory estimation using Scale-ORIGEN and simulating the selected ST-SBO accident using ASTEC, and concluding with JRODOS dispersion analysis around the Peach Bottom unit site. The joint application of the codes provided the opportunity to examine the entire accident in detail and evaluate the results in terms of their impact on public safety.

Regarding the estimation of accident progression ST-SBO, the reference study and ASTEC results showed comparable results for vessel pressure during manual and automatic operation of SRVs. After actuation of ADS and structural degradation, the estimates for vessel failure and the amount of corium ejected are different. The modeling of the lower plenum and the amount of structural mass defined there resulted in inconsistent times for MELCOR and ASTEC. However, the amount of fission products released into the environment is of the same order of magnitude. The transport of fission products from the core to the environment through the CESAR volumes and CPA zones shows consistent results compared to the reference work. A lower plenum definition and mass adjustment could result in simulation results similar to the MELCOR study. To extend the severe accident analysis of the BWR design with ASTEC, new types of fuel assemblies with water rods and a different design and amount of active fuel material can be considered.

To perform a comprehensive analysis of the effects of the received dose, the number of affected meshes must be higher and the simulation period should be larger. Only 24 h of simulations are not sufficient to draw an accurate conclusion. In addition, the calculations in this study did not consider the countermeasures that are important for public safety when fission products are released into the atmosphere. The possible dispersal pathways of fission products through soil and water supply, as well as contamination of food and feed, are also issues that need to be subjected to detailed analysis. Statistical analysis has also shown that some residences, although more distant than other affected areas, have a higher risk of fission product transmission and could have a higher dose rate. The annual regime of winds and rain plays an important role in this case, and statistical analysis can provide clues as to which area has a higher probability of fission products. A decision based on the distance between the power plant and the residential area may not provide enough information to interpret the probability of a dose record in this region. Simulating the statistical analysis for 3–5 years of meteorological data can provide information on which meshes to consider. Detailed analysis considering longer simulation periods and long-term effects of received doses will produce better estimates of public health and safety.

Conducting a severe accident analysis for a BWR design is a step toward expanding the scope of ASTEC. Although the ASTEC code has already implemented boiling water reactor design, the inclusion of BWR-specific fuel channel structures and subchannel physical phenomena, and the evaluation of the results, demonstrates the capabilities of the code in addition to the studies mostly performed at PWR design. A first complementary analysis of a BWR design with ASTEC considering an appropriate fission product inventory, latest physical models and a dispersion study showed promising results for further BWR studies with ASTEC.

CRediT authorship contribution statement

Onur Murat: Methodology, Software, Writing – original draft, Visualization. **Victor Sanchez-Espinoza:** Supervision, Writing – review & editing. **Fabrizio Gabrielli:** Supervision, Writing – review & editing. **Robert Stieglitz:** Supervision. **Cesar Queral:** Supervision, Writing – review & editing.

Declaration of Competing Interest

The authors declare that they have no known competing financial interests or personal relationships that could have appeared to influence the work reported in this paper.

Data availability

The authors do not have permission to share data.

Acknowledgement

Authors would like to thank Alexandre Bleyer, Lionel Chailan, Patrick Chatelard, Patrick Drai, Laurent Laborde and IRSN ASTEC Team; Wolfgang Hering and Christian Staudt for their helps and continues supports. The corresponding author is funded by Republic of Turkey Ministry of National Education during his Ph.D. studies.

References

Adroguer, B., et al., 2003. Core Loss During a Severe Accident (COLOSS Project), COLOSS Final Extended Report, Part 1. IRSN, Experimental and analytical activities Main outcomes from the project, s.l.

Carbajo, J.J., 1994. MELCOR sensitivity studies for a low-pressure, short-term station blackout at the Peach Bottom plant. Nuclear Engineering and Design 152, 287–317.

Carbajo, J., 1993. *Severe Accident Source Term Characteristics for Selected Peach Bottom Sequences Predicted by the MELCOR Code, NUREG/CR-5942,* Oak Ridge, TN 37831-6285: U.S. Nuclear Regulatory Commission.

Chatelard, P., et al., 2016. Main modelling features of the ASTEC V2.1 major version. Annals of Nuclear Energy 93, 83–93.

Chatelard, P. et al., 2017. *Contribution of ASTEC numerical simulations to the understanding of the Fukushima accidents,* Vienna: IAEA Workshop on Advances in Understanding the Progression of Severe Accidents in Boiling Water Reactors.

Epri, 2010. MAAP4 Applications Guidance, Desktop Reference for Using MAAP4 Software, Revision 2. Electric Power Research Institute, Palo Alto, CA.

Hu, J., Gauld, I. C., Peterson, J. L. & Bowman, S. M., 2016. *US Commercial Spent Nuclear Fuel Assembly Characteristics: 1968-2013, NUREG/CR-7227,* Oak Ridge, TN 37831-6170: U.S. Nuclear Regulatory Commission.

Humphries, L. et al., 2017. *MELCOR Computer Code Manuals, Vol. 1: Primer and Users' Guide, Verson 2.2.9541,* Albuquerque: Sandia National Laboratories.

Ievdin, I., Trybushnyi, D., Zheleznyak, M., Raskob, W., 2010. RODOS re-engineering: aims and implementation details. Radioprotection 45, 181–189.

Kolaczkowski, A. M. et al., 1989. *Analysis of Core Damage Frequency: Peach Bottom, Unit 2 Internal Events, NUREG/CR-4550 Vol. 4,* Albuquerque: Sandia National Laboratories.

Larsen, N., 1978. Core Design and Operating Data for Cycles 1 and 2 of Peach Bottom 2, NP-563. General Electric Company, California.

Leonard, M. T., Gauntt, R. O. & Powers, D. A., 2007. *Accident Source Terms for Boiling Water Reactors with High Burnup Cores Calculated Using MELCOR 1.8.5,* Albuquerque: Sandia National Laboratories.

Leonid, A.B., Kirill, S.D., Arkady, E.K., Valery, F.S., 2019. Results of SOCRAT code development, validation and applications for NPP safety assessment under severe accidents. Nuclear Engineering and Design 341, 326–345.

Murat, O., Espinoza, V.S., Wang, S., Stuckert, J., 2020. Preliminary validation of ASTEC V2.2.b with the QUENCH-20 BWR bundle experiment. Nuclear Engineering and Design.

Nagase, F., Uetsuka, H., Otomo, T., 1997. Chemical interactions between B4C and stainless steel at high temperatures. Journal of Nuclear Materials 245 (1), 52–59.

Steinbrück, M., 2010. Degradation and oxidation of B4C control rod segments at high temperatures. Journal of Nuclear Materials 400 (2), 138–150.

U.S. Nuclear Regulatory Commission, 1991. *Radiation Dose Limits for Individual Members of the Public (Subpart D), 10 C.F.R. § 20.1301.* [Online] Available at: [Accessed 16 11 2022].

U.S., Nuclear, Regulatory, Commission, 1990. Severe Accident Risks: An Assessment for Five U.S. Nuclear Power Plants. United States Nuclear Regulatory Commission, NUREG-1150, Washington.

White, J., 1967. Physico-chemical studies of clad UO2 in potential meltdown enviroments. Nuclear Technology Department Nuclear Energy Division General Electric, Virginia.

Wielenberg, A., et al., 2019. Recent improvements in the system code package AC2 2019 for the safety analysis of nuclear reactors. Nuclear Engineering and Design 354, 110211.

Wieselquist, W., Lefebvre, R., Jessee, M., 2020. SCALE Code System, ORNL/TM-2005/39. Oak Ridge National Laboratory, Oak Ridge, TN.